

A. Details of Section 3.1: Benamou-Brenier formulation in Lagrangian coordinates

The Benamou-Brenier formulation of the optimal transportation (OT) problem in Eulerian coordinates is

$$\min_{\mathbf{f}, \rho} \int_0^T \int \|\mathbf{f}(\mathbf{x}, t)\|^2 \rho_t(\mathbf{x}) \, d\mathbf{x} dt \quad (18a)$$

$$\text{subject to} \quad \frac{\partial \rho_t}{\partial t} = -\operatorname{div}(\rho_t \mathbf{f}), \quad (18b)$$

$$\rho_0(\mathbf{x}) = p, \quad (18c)$$

$$\rho_T(\mathbf{z}) = q. \quad (18d)$$

The connection between continuous normalizing flows (CNF) and OT becomes transparent once we rewrite (18) in Lagrangian coordinates. Indeed, for regular enough velocity fields \mathbf{f} one has that the solution of the continuity equation (18b), (18c) is given by $\rho_t = \mathbf{z}(\cdot, t)\#p$ where \mathbf{z} is the flow

$$\dot{\mathbf{z}}(\mathbf{x}, t) = \mathbf{f}(\mathbf{z}(\mathbf{x}, t), t), \quad \mathbf{z}(\mathbf{x}, 0) = \mathbf{x}.$$

The relation $\rho_t = \mathbf{z}(\cdot, t)\#p$ means that for arbitrary test function ϕ we have that

$$\int \phi(\mathbf{x}) \rho_t(\mathbf{x}, t) \, d\mathbf{x} = \int \phi(\mathbf{z}(\mathbf{x}, t)) p(\mathbf{x}) \, d\mathbf{x}$$

Therefore (18) can be rewritten as

$$\min_{\mathbf{f}} \int_0^T \int \|\mathbf{f}(\mathbf{z}(\mathbf{x}, t), t)\|^2 p(\mathbf{x}) \, d\mathbf{x} dt \quad (19a)$$

$$\text{subject to} \quad \dot{\mathbf{z}}(\mathbf{x}, t) = \mathbf{f}(\mathbf{z}(\mathbf{x}, t), t), \quad (19b)$$

$$\mathbf{z}(\mathbf{x}, 0) = \mathbf{x}, \quad (19c)$$

$$\mathbf{z}(\cdot, T)\#p = q. \quad (19d)$$

Note that ρ_t is eliminated in this formulation. The terminal condition (18d) is trivial to implement in Eulerian coordinates (grid-based methods) but not so simple in Lagrangian ones (19d) (grid-free methods). To enforce (19d) we introduce a penalty term in the objective function that measures the deviation of $\mathbf{z}(\cdot, T)\#p$ from q . Thus, the penalized objective function is

$$\int_0^T \int \|\mathbf{f}(\mathbf{z}(\mathbf{x}, t), t)\|^2 p(\mathbf{x}) \, d\mathbf{x} dt + \frac{1}{\lambda} \operatorname{KL}(\mathbf{z}(\cdot, T)\#p \parallel q), \quad (20)$$

where $\lambda > 0$ is the penalization strength. Next, we observe that this objective function can be written as an expectation with respect to $\mathbf{x} \sim p$. Indeed, the Kullback-Leibler divergence is invariant under coordinate transformations, and therefore

$$\begin{aligned} \operatorname{KL}(\mathbf{z}(\cdot, T)\#p \parallel q) &= \operatorname{KL}(p \parallel \mathbf{z}^{-1}(\cdot, T)\#q) = \operatorname{KL}(p \parallel p_\theta) \\ &= \mathbb{E}_{\mathbf{x} \sim p} \log \frac{p(\mathbf{x})}{p_\theta(\mathbf{x})} \\ &= \mathbb{E}_{\mathbf{x} \sim p} \log p(\mathbf{x}) - \mathbb{E}_{\mathbf{x} \sim p} \log p_\theta(\mathbf{x}) \end{aligned}$$

Hence, multiplying the objective function in (20) by λ and ignoring the \mathbf{f} -independent term $\mathbb{E}_{\mathbf{x} \sim p} \log p(\mathbf{x})$ we obtain an equivalent objective function

$$\mathbb{E}_{\mathbf{x} \sim p} \left\{ \lambda \int_0^T \|\mathbf{f}(\mathbf{z}(\mathbf{x}, t), t)\|^2 \, dt - \log p_\theta(\mathbf{x}) \right\} \quad (21)$$

Finally, if we assume that $\{\mathbf{x}_i\}_{i=1}^N$ are iid sampled from p , we obtain the empirical objective function

$$\frac{\lambda}{N} \sum_{i=1}^N \int_0^T \|\mathbf{f}(\mathbf{z}(\mathbf{x}_i, t), t)\|^2 \, dt - \frac{1}{N} \sum_{i=1}^N \log p_\theta(\mathbf{x}_i) \quad (22)$$

B. Additional results

Here we present additional generated samples on the two larger datasets considered, CelebA-HQ and ImageNet64. In addition bits/dim on clean images are reported in Table 2.

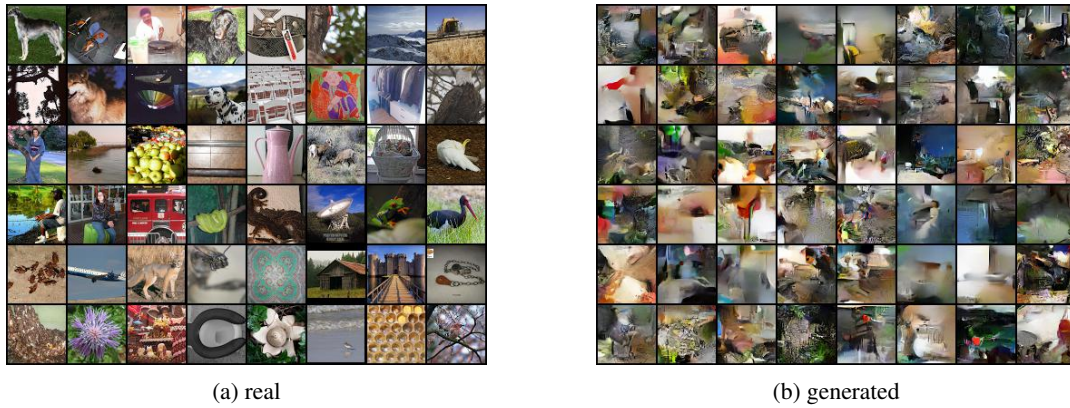


Figure 7. Quality of FFIJORD RNODE generated images on ImageNet-64.

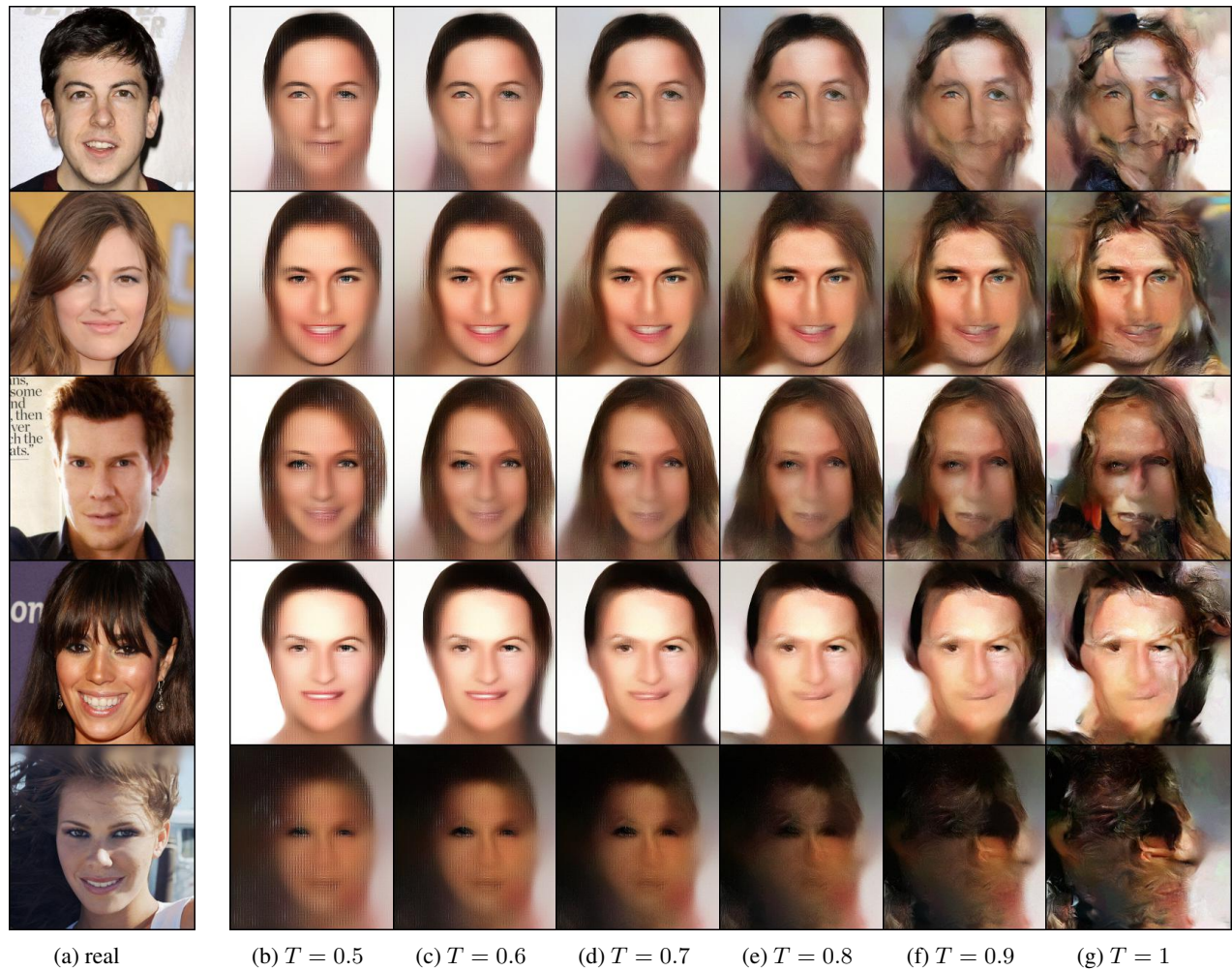


Figure 8. Quality of FFIJORD RNODE generated images on CelebA-HQ. We use temperature annealing, as described in (Kingma & Dhariwal, 2018), to generate visually appealing images, with $T = 0.5, \dots, 1$.

Table 2. Additional results and model statistics of FFJORD RNODE. Here we report validation bits/dim on both validation images, and on validation images with uniform variational dequantization (ie perturbed by uniform noise). We also report number of trainable model parameters.

DATASET	BITS/DIM (CLEAN)	BITS/DIM (DIRTY)	# PARAMETERS
MNIST	0.92	0.97	8.00e5
CIFAR10	3.25	3.38	1.36e6
IMAGENET64	3.72	3.83	2.00e6
CELEBA-HQ256	0.72	1.04	4.61e6